The Pennsylvania State University

The Graduate School

Department of Geosciences

INVESTIGATING THE IMPACT OF ADVECTIVE AND DIFFUSIVE CONTROLS IN SOLUTE TRANSPORT ON GEOELECTRICAL DATA

A Thesis in

Geosciences

by

Daniel D. Wheaton

Submitted in Partial Fulfillment
of the Requirements
for the Degree of

Master of Science

May 2009

The thesis of Daniel D. Wheaton was reviewed and approved* by the following:

Kamini Singha
Assistant Professor of Geosciences
Thesis Advisor

Andy Nyblade
Professor of Geosciences

Demian Saffer
Associate Professor of Geosciences

Katherine H. Freeman
Professor of Geosciences
Associate Head of Graduate Programs

*Signatures are on file in the Graduate School

ABSTRACT

Multiple types of physical heterogeneity have been suggested to explain anomalous solute transport behavior, yet determining exactly what controls transport at a given site is difficult from concentration histories alone. Differences in timing between co-located fluid and bulk apparent electrical conductivity data have previously been used to estimate solute mass transfer rates between mobile and less mobile domains; here, we consider if this behavior can arise from other types of heterogeneity. Numerical models are used to investigate the electrical signatures associated with large-scale hydraulic conductivity heterogeneity and small-scale dual-domain mass transfer, and address issues regarding the scale of the geophysical measurement. We examine the transport behavior of solutes with and without dual-domain mass transfer, in: 1) a homogeneous medium, 2) a discretely fractured medium, and 3) a hydraulic conductivity field generated with sequential Gaussian simulation. We use the finite element code COMSOL Multiphysics to construct two-dimensional cross-sectional models and solve the coupled flow, transport, and electrical conduction equations.

Our results show that both large-scale heterogeneity and subscale heterogeneity described by dual-domain mass transfer produce a measurable hysteresis between fluid and bulk apparent electrical conductivity, indicating a lag between changes in the mobile and less mobile domains of an aquifer, or mass transfer processes, at some scale. The shape and magnitude of the observed hysteresis is controlled by the spatial distribution of hydraulic heterogeneity, mass transfer rate between domains, and the ratio of mobile to immobile porosity. Because the rate of mass transfer is related to the inverse square of a diffusion length scale, our results suggest that the shape of the hysteresis curve is indicative of the length scale over which mass transfer is occurring. We also demonstrate that the difference in scale between fluid conductivity and geophysical measurements is not responsible for the observed hysteresis. We suggest that there is

a continuum of hysteresis behavior between fluid and bulk electrical conductivity caused by mass transfer over a range of scales from small-scale heterogeneity to macroscopic heterogeneity.

TABLE OF CONTENTS

LIST OF FIGURES v

LIST OF TABLES vii

ACKNOWLEDGMENTS viii

Introduction 1

Model Construction 5

- Development of a Homogeneous Model 9
  - Modeling Classical Advective-Dispersive Behavior 10
  - Modeling Dual Domain Mass Transfer 12
- Effects of Averaging and Measurement of Support Volume 14
- Development of a Discrete Fracture Model 15
  - Modeling Classical Advective-Dispersive Behavior 17
  - Modeling Dual Domain Mass Transfer 19
- Development of a Heterogeneous Hydraulic Conductivity Model 21
  - Modeling Classical Advective-Dispersive Behavior 23
  - Modeling Dual Domain Mass Transfer 25

Discussion and Model Relevance to Field Studies 27

Conclusions 29

Appendix A Future Work 30

Appendix B Using COMSOL Multiphysics for Modeling Coupled Systems 32

Appendix C Scripting a Homogeneous Dual-Domain Mass Transfer Model 37

References 46

LIST OF FIGURES

Figure 1: Conceptual model of dual-domain mass transfer. Solute moves through two domains: the mobile zone or continuous pathway and the immobile zone or discontinuous pathway. The mass transfer rate controls the diffusive exchange of solute between the two domains. In the example on the left, the fracture represents the mobile zone while the matrix represents the immobile zone. In the example on the right, solute following the path of the solid white line would move through the mobile zone. Solute following the dotted white path would move into dead-end pore space or immobile zone and have to diffuse back into the mobile zone. 2

Figure **2**: Simulated bulk apparent and fluid EC for a model with homogeneous hydraulic conductivity. The black line is the true relation between bulk apparent and fluid EC used in the model. The simulated bulk apparent EC deviates from the true value as a function of support volume or geometric factor, but does not produce a measurable hysteresis when dual-domain mass transfer is not simulated (black symbols). Introducing dual-domain mass transfer at a rate of 10^{-3}/day (gray symbols) produces hysteresis. During the injection and storage periods, the hysteresis curve is below the true relation between fluid and bulk apparent EC because the immobile domain, which accounts for 75% of the total porosity of 0.1, is relatively fresh compared to the mobile domain. Although not shown here, the shape of the hysteresis is controlled by the rate of mass transfer and ratio of mobile to immobile porosity..... 11

Figure **3**: (a) Mobile and (b) immobile concentrations through time from a model with homogeneous hydraulic conductivity at one point in space. Lower concentration peaks in the mobile zone exist for models with dual-domain mass transfer. The decrease in mobile porosity from the model without dual-domain mass transfer (10% porosity) to the model with dual-domain mass transfer (2.5% porosity) causes a corresponding increase in transport velocity resulting in earlier solute arrival times in the dual-domain mass transfer model; for the same reason, tailing behavior is comparatively suppressed. At high (10^{-1}/day) or low (10^{-3}/day) mass-transfer rates, the mobile and immobile domains approach equilibrium and behavior is similar to a single domain model. Deviation in equilibrium behavior is notable at intermediate mass transfer rates..... 13

Figure **4**: Mesh used in the fracture at 36-m depth and in the vicinity of the pumping/injection and observation wells. Well locations are white and electrodes are represented with black rectangles. 15

Figure **5**: (a) Mobile and (b) immobile concentrations from a point within the discrete fracture. Without dual-domain mass transfer, concentration rebound is observed at the beginning of the pumping period due to solute being pulled back through the fracture. Introducing dual-domain mass transfer (thus lowering the mobile porosity from 0.1 to 0.025, in these models) hastens solute arrival times. With dual-domain mass transfer, lower peak concentrations and longer tails are observed. (c) Mobile domain concentrations for models with a homogenous mass transfer rate versus those with differing mass transfer rates between the matrix and fracture are nearly identical. 18

Figure **6**: Simulated bulk apparent and fluid EC for with a point within the discrete fracture. The black line is the true relation between bulk apparent and fluid EC used in the model. Discrete fracture zones result in hysteresis between bulk and fluid EC without explicitly invoking mass transfer processes (black symbols). Introducing dual-domain mass transfer increases the hysteresis (grey symbols). During the injection period, the hysteresis curve in the presence of dual-domain mass transfer is below the true relation between fluid and bulk apparent EC because the immobile domain (7.5% porosity) is relatively fresh compared to the mobile domain (2.5% porosity).....19

Figure **7**: Mesh used in the heterogeneous K-field simulations in the vicinity of the pumping/injection and observation wells. Well locations are white and electrodes are represented with black rectangles.....22

Figure **8**: (a) Mobile and (b) immobile concentration at one point in space from the model with heterogeneous hydraulic conductivity. Although solute plume snapshots (not shown here) demonstrate preferential pathways, solute behavior in the mobile domain is similar to the homogeneous case. Introducing dual-domain mass transfer (thus lowering the mobile porosity from 0.1 to 0.025, in these models) hastens solute arrival times and tailing behavior similar to the homogeneous case. At low (10^{-3}/day) or high (10^{-1}/day) mass transfer rates, the mobile and immobile domains approach equilibrium and concentration behavior is similar to the single domain case. Intermediate transfer rates result in deviation from equilibrium behavior such as the rebound observed at the beginning of the pumping period. With dual-domain mass transfer, mobile domain concentration peaks are lower and longer tails are observed.....24

Figure **9**: Simulated bulk apparent and fluid EC for a model with heterogeneous hydraulic conductivity. The black line is the true relation between bulk apparent and fluid EC used in the model. Heterogeneity in hydraulic conductivity (var(ln(K) = 1.2), without dual domain mass transfer, results in a slight hysteresis between fluid and bulk apparent EC without invoking mass transfer processes explicitly (black symbols). The addition of dual-domain mass transfer at a rate of 10^{-1}/day (grey symbols) increases the hysteresis, as would be expected. The hysteresis observed here is smaller than the previous two cases because the high rate of mass transfer keeps the mobile and immobile domains closer to equilibrium. 25

LIST OF TABLES

Table **1**: Physical parameters used in the homogeneous numerical models of flow, transport, and electrical conduction. 9

Table **2**: Physical parameters used in the discrete fracture numerical models of flow, transport, and electrical conduction. 16

Table **3**: Physical parameters used in the heterogeneous numerical models of flow, transport, and electrical conduction. 22

ACKNOWLEDGMENTS

I would like to thank Kamini Singha for being an enthusiastic collaborator on this project from start to finish. I am also grateful to Derek Elsworth for enlightening modeling discussions. I appreciate the lively discussions of the hydro-tectonics group. Specifically, my discussions with Christine Regalla, Maggie Popek, and Brad Kuntz always gave me fresh insight into my own work.

Although the field work I conducted is not presented here, it was an important experience that gave me a valuable perspective on my research. For that, I thank the staff at the USGS Office of Groundwater, Branch of Geophysics, including Carole Johnson, Fred Day-Lewis, Rory Henderson, and Yongping Chen for allowing me access to the field site and pertinent data, as well as assistance in the field. I also thank Nicholas Rubert, who was an invaluable field assistant.

Most importantly, I thank my friends and family – their continued support made this work possible.

This work was funded by American Chemical Society PRF Grant 45206-G8 and NSF grant EAR-0747629.

Introduction

Subsurface solute transport is classically described with the advection-dispersion equation, which assumes that transport is Fickian in nature, such that concentration observed over time at a point in space (known as a concentration history or breakthrough curve) has a nearly Gaussian distribution for a conservative solute [*Bear* 1972; *Berkowitz and Scher* 2001]. Breakthrough curves from laboratory and field experiments over the past several decades, however, often exhibit anomalous behavior, including skewed curves, elongated tails, and/or multiple peaks [e.g., *Adams and Gelhar* 1992; *Levy and Berkowitz* 2003; *Cortis and Berkowitz* 2004]. Numerous hypotheses exist for describing this behavior, including diffusion-like processes such as dual-domain mass transfer [e.g., *Haggerty and Gorelick* 1994, 1995], time delays between the concentration gradient and mass flux from inertial effects and subscale heterogeneity [e.g., *Dentz and Tartakovsky* 2006], and variable transport rates caused by large-scale heterogeneity [e.g., *Becker and Shapiro* 2000, 2003]. Several mathematical formulations such as continuous-time random-walk theory [e.g., *Berkowitz and Scher* 1995] and fractional advection-dispersion equations [e.g., *Benson et al.* 2000] have been proposed to simulate these observed transport behaviors.

Diffusion-based processes in dual domains have been thought to control transport in some settings. For example, an advection-dispersion model could not explain all the salient features of the bromide plume, most notably the mass balance, during a tracer test in the fluvial materials at the MAcroDispersion Experiment (MADE) Site in Columbus, Mississippi. At early time, the plume mass was overestimated by 52% while at late times it was underestimated by 23% [*Adams and Gelhar* 1992]. Numerical simulations utilizing dual-domain mass transfer, where solute diffuses between a mobile zone (the continuous path, such as fractures or connected

pore space) and an immobile or less-mobile zone (a discontinuous path, such as the rock matrix surrounding fractured media, or unconnected pore space), was able to accurately predict both solute migration and mass balance characteristics at the MADE site [*Feehley et al.* 2000; *Harvey and Gorelick* 2000]. Transport models controlled by advection-dispersion only were unable to explain the same behavior [*Barlebo et al.* 2004].

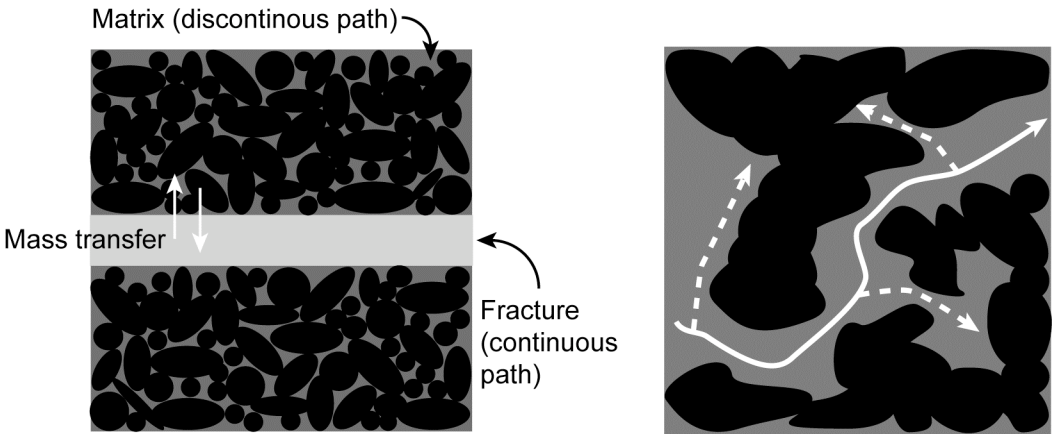

Figure 1: Conceptual model of dual-domain mass transfer modified. Solute moves through two domains: the mobile zone or continuous pathway and the immobile zone or discontinuous pathway. The mass transfer rate controls the diffusive exchange of solute between the two domains. In the example on the left, the fracture represents the mobile zone while the matrix represents the immobile zone. In the example on the right, solute following the path of the solid white line would move through the mobile zone. Solute following the dotted white path would move into dead-end pore space or immobile zone and may have to diffuse back into the mobile zone.

Other studies have explained anomalous solute tailing behavior using advectively controlled transport. For example, tracer tests were conducted in a fractured-rock environment at Mirror Lake, New Hampshire, using three separate conservative tracers with different diffusion coefficients, each with two different pumping configurations [*Becker and Shapiro* 2000, 2003]. Because tracers with different diffusion coefficients produced identical late-time breakthrough behavior, the authors concluded that long tailing resulted from an advective mechanism, not a

diffusive one, and proposed that the solute advects via different paths at different speeds to reach a given destination. The early arrivals represent solute that has taken the fastest route whereas the later arrivals have taken a longer way or slower path; the authors termed this behavior "heterogeneous advection". *Day-Lewis et al.* [2006] supported these results by collecting a suite of saline tracer, hydraulic and time-lapse radar data at Mirror Lake, and demonstrated that heterogeneity in the permeability structure could explain their field observations. In highly heterogeneous material such as fractured rock, anomalous transport controlled by advection is an attractive explanation.

Distinguishing between the processes controlling transport, such as heterogeneous advection based on macroscopic heterogeneity versus diffusive processes like dual-domain mass transfer, is generally based on solute concentration histories measured within the mobile domain. Unfortunately, concentration histories often do not contain enough information to distinguish between the proposed processes. *Sánchez-Vila and Carrera* [2004] demonstrated that for large travel distances breakthrough-curve shape could not be used to discern between advectively controlled and diffusion-controlled transport because it is possible to choose physical parameters for both conceptual models that resulted in each one fitting the same set of temporal moments. There is consequently still some question as to when a simple advection-dispersion model should be used to reproduce the plume characteristics [*Barlebo et al.* 2004; *Hill et al.* 2006; *Molz et al.* 2006] and over what length scale mass transfer occurs. To accurately predict solute migration through natural systems, we must integrate new data types that may help to discriminate which processes control solute transport, and determine which models are most appropriate at a particular field site.

Geophysical methods may provide additional pertinent data in these investigations. Results from an electrical geophysical dataset obtained during an aquifer-storage and recovery (ASR) test in Charleston, South Carolina indicate that direct-current resistivity methods may be

able to help estimate mass transfer behavior in situ [*Singha et al.* 2007]. The authors observed hysteresis between fluid electrical conductivity (EC) and the bulk apparent EC, which contradicts common rock physics relations, and suggested that the hysteresis is an effect of dual-domain mass transfer. They contended that the lag between fluid EC and bulk apparent EC is controlled by the rate of transfer between mobile and immobile zones. This observation indicates that electrical geophysical data, in conjunction with saline tracer tests, may provide evidence about scales of mass transfer in controlling solute breakthrough behavior. This conclusion was further supported by theoretical work in *Day Lewis and Singha* [2008] and *Singha et al.* [2008].

To discriminate the processes controlling transport with geophysical methods, we need to quantify the "footprint" or support volume of the geophysical measurement. If the fluid and bulk EC data are out of equilibrium solely due to differences in support volume, then plume shape could play an important role in the interpretation of the hysteresis between bulk and fluid EC, as previous studies have shown that large, diffuse plumes can be more easily captured with electrical data than small, highly concentrated ones [*Singha and Gorelick* 2006]. If averaging by the geophysical method is not responsible for the disequilibrium between bulk apparent and fluid EC data, then the observed disequilibrium suggests the effect of either dual-domain mass transfer or heterogeneous advection. Geophysical data can then be used to monitor disequilibrium between subsurface domains at some effective scale. No studies have looked at this effect in detail.

Here, we use numerical models to investigate the electrical signatures of solutes associated with large-scale permeability heterogeneity and dual-domain mass transfer to determine if the behavior in geophysical data is dependent on the scale of heterogeneity or process controlling solute transport. These numerical models highlight how differences in scale and support between hydrologic and geophysical methods affect data interpretation. Below, we analyze a series of numerical experiments to understand the impact macroscopic hydraulic

conductivity heterogeneity and dual-domain mass transfer have on breakthrough curves and electrical signatures.

Model Construction

To test how macroscopic permeability heterogeneity and dual-domain mass transfer control solute tailing behavior for simplified situations and how these processes are detected with electrical data, a coupled flow, transport and electrical conduction numerical model was constructed using COMSOL Multiphysics [*COMSOL Multiphysics User's Guide* 2006]. Two-dimensional, transient cross-sectional models were created to investigate solute transport from an injection well in the presence and absence of dual-domain mass transfer under a variety of geologic conditions, including: 1) homogeneous hydraulic conductivity in the subsurface, 2) discretely fractured media, and 3) highly heterogeneous hydraulic conductivity without discrete fractures in the subsurface. Hydraulic head, solute concentration, and bulk apparent EC data were simulated for each conceptual model.

We first solve a transient flow system described by:

$$S\frac{\partial H}{\partial t}+\nabla\cdot[-\frac{K}{(\rho_f g)}\nabla(p+\rho_f gD)]=Q_S \tag{1}$$

$$H=\frac{p}{(\rho_f g)}+D \tag{2}$$

where S is the storage term (1/L), H is hydraulic head (L), t is time (T), K is the hydraulic conductivity (L/T), ρ_f is the fluid density (M/L^3), g is the constant of gravitational acceleration (L/T^2), p is the pressure (M/LT^2), D is elevation (L), and Q_S is the source of fluid (1/T). For a single domain, the predicted flow velocities from this numerical model are used to solve for concentration by:

$$\Phi_m\frac{\partial c_m}{\partial t}+\nabla\cdot(-\Phi_m D_L\nabla c_m)=-\mathbf{u}\nabla c_m+R_L \tag{3}$$

where Φ_m is the connected porosity (dimensionless), c_m is the solute concentration in the connected pore space (M/L^3), t is time (T), D_L is the coefficient of hydrodynamic dispersion (L^2/T), **u** is the fluid velocity vector (L/T), and R_L is the chemical reaction of the solute in the liquid phase (M/L^3T). The form of the coefficient of hydrodynamic dispersion is:

$$D_{ii} = \alpha_L \frac{\mathbf{u}_i^2}{\overline{\mathbf{u}}} + \alpha_T \frac{\mathbf{u}_j^2}{\overline{\mathbf{u}}} + \tau_L D_{mL} \tag{4a}$$

$$D_{ji} = D_{ij} = (\alpha_L - \alpha_T) \frac{\mathbf{u}_i \mathbf{u}_j}{\overline{\mathbf{u}}} \tag{4b}$$

where α_L is the dispersivity in the longitudinal flow direction (L), α_T is the dispersivity in the transverse flow direction (L), $\mathbf{u}_i$ are the fluid velocity components in the respective directions, τ_L is the tortuosity factor (dimensionless), and D_{mL} is the coefficient of molecular diffusion of the solute (L^2/T).

For models incorporating dual-domain mass transfer, a second equation describes that process:

$$\Phi_{im} \frac{\partial c_{im}}{\partial t} + \nabla \cdot (-\Phi_{im} D_L \nabla c_{im}) = R_L \tag{5}$$

where Φ_{im} is the immobile porosity (dimensionless) and c_{im} is the solute concentration in the immobile domain (M/L^3). In this case, the hydrodynamic dispersion term only includes molecular diffusion. The reaction term links the mobile and immobile domains, where

$$\text{for the mobile domain: } R_L = \beta(c_m - c_{im}), \text{ and} \tag{6a}$$

$$\text{for the immobile domain: } R_L = -\beta(c_m - c_{im}) \tag{6b}$$

where β is the rate of diffusive mass transfer between domains (1/T). We note that for the models here, only a single rate of mass transfer is used, although previous studies have used

multi-rate models to account for mass transfer rates that vary with scale [e.g., *Haggerty and Gorelick* 1995].

To convert estimated concentrations to electrical conductivity, we follow the relation established in *Keller and Frischknecht* [1966] where 1 mg/L equals 0.002 mS/cm. For models without dual-domain mass transfer, the fluid EC can be used in Archie's Law [*Archie* 1942] to calculate the bulk EC:

$$\sigma_b = a\sigma_f \Phi_m^{\eta} \tag{7}$$

where a is a fitting parameter (dimensionless), σ_f is the fluid conductivity (mS/cm), and η is the cementation exponent (dimensionless), which is related to the geometry of the pore-space and typically ranges between 1.8 and 2. In the models with dual-domain mass transfer, we follow *Singha et al.* [2007] to calculate the bulk EC:

$$\sigma_b = (\Phi_m + \Phi_{im})^{\eta-1} \cdot (\Phi_m \sigma_{f,m} + \Phi_{im} \sigma_{f,im}) \tag{8}$$

where $\sigma_{f,m}$ is the fluid conductivity in the mobile domain (mS/cm) and $\sigma_{f,im}$ is the fluid conductivity in the immobile domain (mS/cm). Bulk EC were then used to solve for voltage using the following equation:

$$-\nabla \cdot d(\sigma_b \nabla V - J^e) = dQ_j \tag{9}$$

where d is the thickness in the third direction into the page for these 2-D models (L), V is the electric potential (volts), J^e is the external current density (A/L^2), and Q_j is the current source (A/L^3). The electric potential is used to calculate the bulk apparent EC:

$$\sigma_{ba} = \frac{I}{(V_M - V_N) \cdot K_F} \tag{10}$$

where V_M is the electric potential at the first potential electrode (volts), V_N is the electric potential at the second potential electrode (volts), K_F is the geometric factor (L), and I is the current (A).

The model domain is 60 m tall by 100 m wide, and includes an internal area of fine meshing near the injection well and electrode locations. An unstructured triangular mesh was generated using the free mesher and a predefined coarse mesh size, and was then refined. The maximum element growth rate was 50%. The top and bottom boundaries for the flow and transport simulations are no flux boundaries. For flow, the left boundary is a specified head of 3 m, and the right boundary is a specified head of 1 m, producing a hydraulic head gradient of 0.02. For transport, the left boundary is a specified concentration of 85 mg/L. The right-hand boundary is an advective-flux condition, which allows any solute being carried by the fluid to exit the model, preventing a buildup of solute at the boundary. The background concentration was set to 85 mg/L. When dual-domain mass transfer exists within the model, the initial concentration in the immobile domain was also set to 85 mg/L. For electrical flow, all boundaries were set to electric potential of 0 V. Parameters used in the modeling are shown in Table 1.

To evaluate the electrical response to tracer behavior, we simulate a push-pull type test, loosely mimicking the data collection procedure described in *Singha et al*. [2007]. The injection/extraction well was represented by a series of 32 points spaced 1 m apart vertically from 9 m to 40 m below the simulated land surface and 46.5 m to the right of the model origin, near the midpoint of the system. At these locations, we injected 16 g/L of solute at a total rate of 0.07 L/s for 12 days, then ended the injection and allowed the fluid to flow due to the head gradient imposed by the boundary conditions for 2 days, and then extracted fluid at a total rate of 0.095 L/s for 32 days. The injection and pumping rates mentioned above were distributed evenly among the points representing the active well to evenly distribute the pressure and solute over the entire well. Another series of 24 points located 7 m to the right of the injection well and spaced 1 m apart vertically from 17 m to 40 m below the simulated ground surface represent the observation well and electrodes. To drive current, a given electrode pair was simulated by giving

one point at the observation well a current source of 1 A/m and giving the other one a current source of -1 A/m.

Bulk apparent EC measurements were simulated with a dipole-dipole type array considering only in-well dipoles. Skip-0 to skip-2 geometries were used, where the 'skip' describes how many electrodes were skipped within a dipole; for a smaller skip, the measurement averages less of the subsurface and provides better resolution [*Slater et al.* 2000]. We consider raw, uninverted bulk apparent EC data in this study, as was done in *Singha et al*. [2007], where apparent EC values are calculated using the injected current, voltage change between potential electrodes, and a theoretically calculated geometric factor.

Flow and transport both required transient analysis because the injection and pumping conditions are time dependent. Because the bulk apparent EC measurement and its effects are effectively instantaneous, the electrical flow only required a steady-state analysis. The flow and transport problems were solved simultaneously (strongly coupled). In the presence of dual-domain mass transfer, the second transport equation is solved as strongly coupled with the flow and transport problem. After the flow and transport simulations were finished, the steady-state electrical equation was solved through time for all the different electrode configurations. The models simulate a total of 1100 hours to capture the extent of the tailing.

Development of a Homogeneous Model

To start, we consider a numerical model given the boundary and initial conditions outlined above with a homogeneous hydraulic conductivity of 1.15×10^{-4} m/s. In this system, we model both classic advective-dispersive behavior and dual-domain mass transfer, and explore the geophysical signature associated with both. This model mesh was refined until the element sides were approximately 17 cm long, and ended up containing 8491 triangular elements. The models

presented here have a total porosity, in both cases, of 0.1. Modeling parameters are summarized in Table 1.

Table 1: Physical parameters used in the homogeneous numerical models of flow, transport, and electrical conduction.

Storage term (S)	3×10^{-5} m^{-1}
Hydraulic conductivity (K)	1.15×10^{-4} m/s
Hydraulic gradient	0.02
Injection rate	0.07 L/s
Pumping rate	0.095 L/s
Total porosity (Φ_m)	0.1
Dispersivity, primary direction (mobile) (α_1)	1 m
Dispersivity, secondary direction (mobile) (α_2)	0.1 m
Tortuosity factor (τ_L)	1
Coefficient of molecular diffusion (D_L)	1×10^{-6} m^2/s
Initial solute concentration	85 mg/L
Injection concentration	16,000 mg/L
Current driven	1 A/m
Mass transfer rate (β)	1×10^{-3}/day – 1×10^{-1}/day
Mobile porosity (Φ_m)	0.025
Immobile porosity (Φ_{im})	0.075
Dispersivity, primary direction (immobile, α_1)	0 m
Dispersivity, secondary direction (immobile, α_2)	0 m

Modeling Classical Advective-Dispersive Behavior

When modeling classic advective-dispersive behavior, the tracer transport appears Fickian, as expected: skip-0 bulk apparent EC in the homogeneous model behaves in accordance with classical solute transport and Archie's Law, and fluid EC and bulk apparent EC vary linearly (Figure 1). The bulk apparent and fluid EC at the observation well increase over time as solute breaks through, and then decrease during the pumping period as tracer is pulled back to the injection well. Although there is no heterogeneity in this scenario, we find that similar to field bulk EC data, the model results show that as electrode spacing increases, the response associated with the plume decreases. This behavior is expected because increasing the electrode spacing increases the support volume of the measurement at the expense of measurement resolution. Consequently, we deal only with skip-0 data here. However, we note that increasing the skip does not cause a disequilbrium between the fluid and bulk EC data in these models, indicating, at least at the macroscopic scale, that the scale of measurement does not impart hysteresis without the presence of heterogeneity.

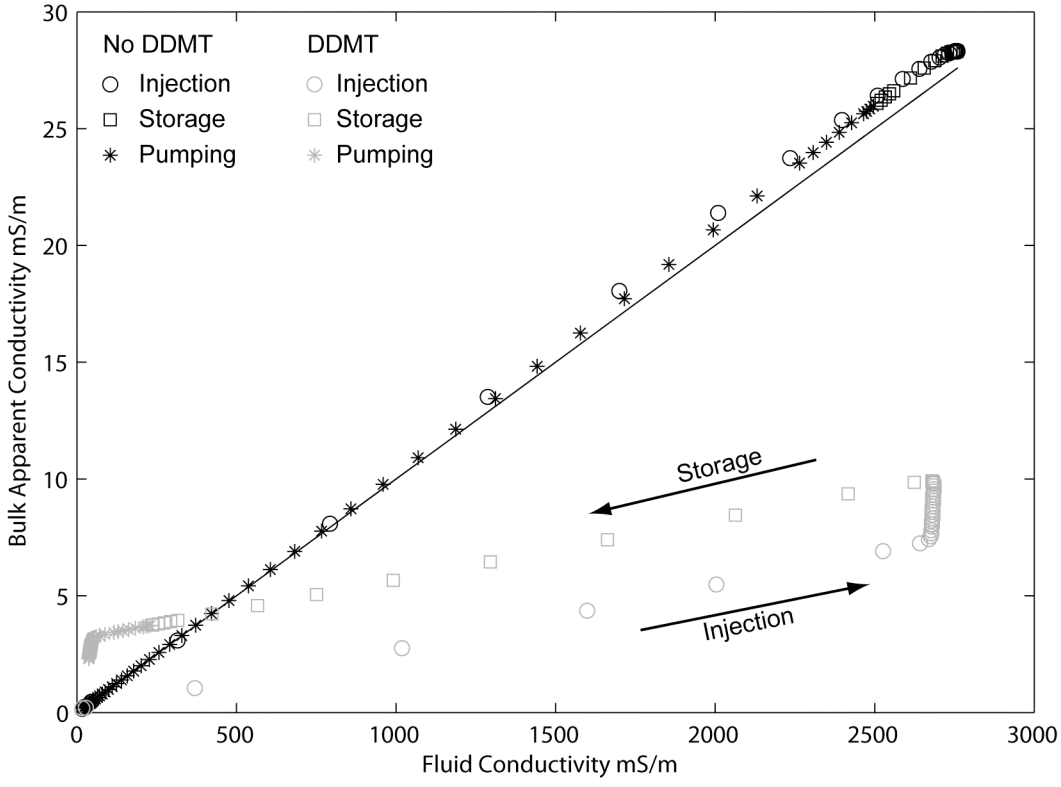

Figure 2: Simulated bulk apparent and fluid EC for a model with homogeneous hydraulic conductivity. The black line is the true relation between bulk apparent and fluid EC used in the model. The simulated bulk apparent EC deviates from the true value as a function of support volume or geometric factor, but does not produce a measurable hysteresis when dual-domain mass transfer is not simulated (black symbols). Introducing dual-domain mass transfer at a rate of 10^{-3}/day (gray symbols) produces hysteresis. During the injection and storage periods, the hysteresis curve is below the true relation between fluid and bulk apparent EC because the immobile domain, which accounts for 75% of the total porosity of 0.1, is relatively fresh compared to the mobile domain. Although not shown here, the shape of the hysteresis is controlled by the rate of mass transfer and ratio of mobile to immobile porosity.

Modeling Dual-Domain Mass Transfer

Given the same parameterization as above, we add dual-domain mass transfer to our simulation. This requires the selection of two additional parameters: immobile porosity and mass transfer rate, as shown in equations 5 and 6. In these models, the immobile porosity is set to be 0.075 and the mobile porosity is set to 0.025, for the same total porosity that was used in the previous simulation. At low mass transfer rates (<1 x 10^{-3}/day), the system behaves as a single domain (Figure 2), and transport is approximately Fickian. At 1 x 10^{-2}/day, the dual-domain behavior is noticeable (Figure 2) and by 1 x 10^{-3}/day, the results are distinct compared to a single domain model—elongated tails exist in the breakthrough curves. The rate of mass transfer is equal to the diffusion divided by the length scale of mass transfer squared, so a mass transfer rate of 1 x 10^{-3}/day is equivalent to heterogeneity on the scale of ~9 m given a diffusion coefficient of 1 x 10^{-6} m^2/s, whereas a mass transfer rather of 1 x 10^{-2}/day is equivalent to heterogeneity on the scale of ~3 m.

Mobile-domain concentrations in injection, storage, and early pumping periods are lower in the presence of dual-domain mass transfer than would be expected in the single domain case due to mass being stored in the less-mobile domain (Figure 2). During the pumping stage, mobile concentrations are higher than in the single-domain model because previously trapped solute is

diffusing back into the mobile domain from an immobile domain "source". For rates of mass transfer greater than 1 x 10^{-3}/day, we observe a concentration rebound at the beginning of the pumping stage (Figure 2) because as the solute concentration in the mobile domain is removed, the mobile domain becomes out of equilibrium with the high solute concentration in the immobile domain. To compensate, a large amount of solute is transferred back into the mobile domain causing the concentration rebound observed in the breakthrough curve.

In the presence of dual-domain mass transfer, fluid and bulk apparent EC show hysteresis (Figure 1). Bulk apparent EC is lower during the injection and early parts of the storage phases than expected from the mobile fluid EC, assuming equation 7, due to the remaining freshwater in the immobile domain, and bulk apparent EC is greater than expected during the pumping and late storage phases as the saline tracer moves into the immobile domain. As the transfer rate is increased, the lag between fluid and bulk EC increases, creating a wider hysteresis curve. However, at sufficiently fast rates (10^{-1}/day; length scale of 0.9 m) the lag is reduced because the two domains equilibrate quickly and again act as a single domain with a total porosity equal to the mobile plus immobile porosities.

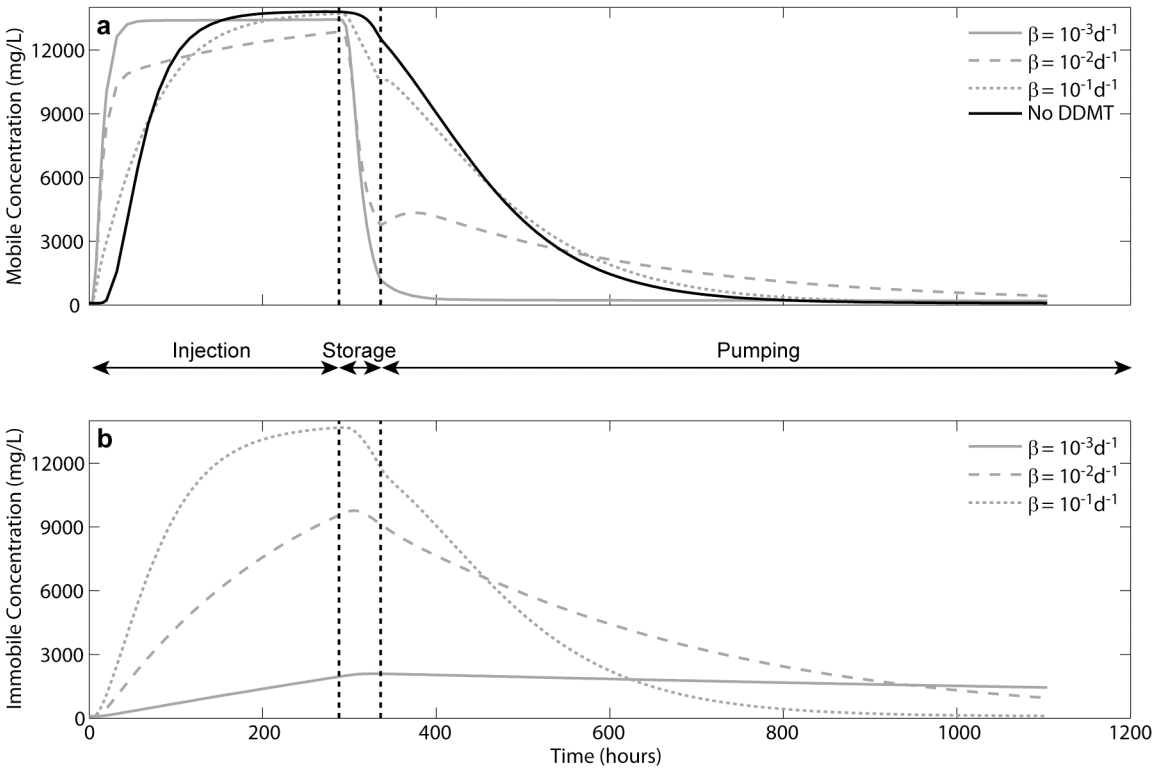

Figure 3: (a) Mobile and (b) immobile concentrations through time from a model with homogeneous hydraulic conductivity at one point in space. Lower concentration peaks in the mobile zone exist for models with dual-domain mass transfer. The decrease in mobile porosity from the model without dual-domain mass transfer (10% porosity) to the model with dual-domain mass transfer (2.5% porosity) causes a corresponding increase in transport velocity resulting in earlier solute arrival times in the dual-domain mass transfer model; for the same reason, tailing behavior is comparatively suppressed. At high (10^{-1}/day) or low (10^{-3}/day) mass-transfer rates, the mobile and immobile domains approach equilibrium and behavior is similar to a single domain model. Deviation in equilibrium behavior is notable at intermediate mass transfer rates.

Effects of Averaging and Measurement of Support Volume

Archie's Law does not account for the fact that geophysical measurements have a larger support volume than the fluid EC, and consequently can 'see' solute that is outside of a sampling well [*Singha and Gorelick* 2006]; there is consequently the possibility that hysteresis is caused solely by a difference in scale between the measurements. To assess the ability of measurement support volume to cause hysteresis in the absence of heterogeneity, we constructed a homogeneous model with a constant background solute concentration of 85 mg/L. Using this model, we calculated the geometric factor for the electrode configurations used above. We then introduced the tracer via the injection/extraction well as described above and using the same electrode configuration, invoked the injection current, and calculated the voltage change, and we observed a deviation between the calculated bulk apparent EC using equation 10 and the bulk apparent EC estimated from the model (Figure 1). We then repeated the experiment for the same background concentration, but varied the injection concentration, thus creating a difference in EC between the background and the plume, which would change the support volume of the measurement as the current paths change. In doing so, we found that the shape of this deviation between the true and calculated bulk apparent EC is consistent for all the injection concentrations. This indicates that the deviation results from a change in the support volume of the measurement

or a change in the geometric factor as a function of the model's deviation from homogeneity—both effects are caused by the evolving plume geometry and cannot be separated—but importantly, no hysteresis between bulk apparent and true EC is seen in any of these models. This means that for the models presented here, the observed hysteresis is caused by transport processes, not the difference in support volume between fluid and bulk apparent EC.

Development of a Discrete Fracture Model

To compare the above results to those from a system in which macroscopic permeability heterogeneity may lead to anomalous transport, we develop a numerical model with a discrete fracture. A planar feature 0.2 m wide was emplaced at a depth of 36 m across the model domain to represent a fractured zone. Except for increasing the hydraulic conductivity within the fracture to 0.01 m/s, all other parameters are the same as in the homogeneous model, including a total assumed porosity of 0.1. The rate of mass transfer (β) is the same in both the fracture and matrix. An unstructured triangular mesh was sequentially generated outward, resulting in element properties similar to that of the homogeneous model; however, due to the small elements within the fracture, this model contained 17669 triangular elements (Figure 3). Model parameters are summarized in Table 2.

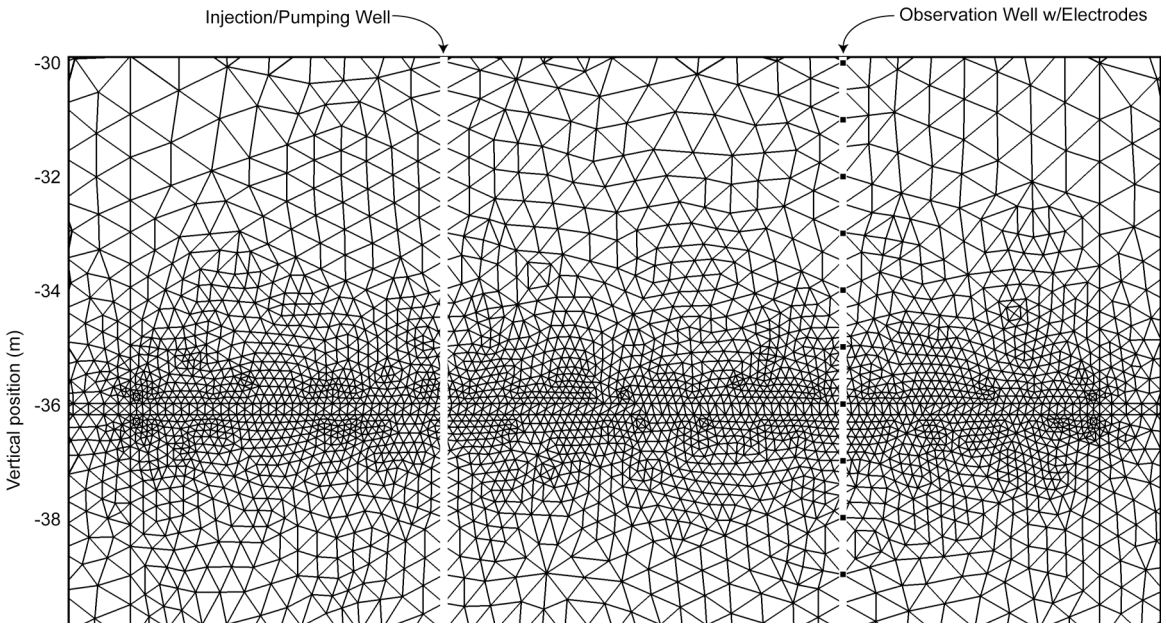

Figure 4: Mesh used in the fracture at 36-m depth and in the vicinity of the pumping/injection and observation wells. Well locations are white and electrodes are represented with black rectangles.

Table 2: Physical parameters used in the discreet fracture numerical models of flow, transport, and electrical conduction.

Storage term (S)	3×10^{-5} m^{-1}
Hydraulic conductivity, fracture (K)	1×10^{-2} m/s
Hydraulic conductivity (K)	1.15×10^{-4} m/s
Hydraulic gradient	0.02
Injection rate	0.07 L/s
Pumping rate	0.095 L/s
Total porosity (Φ_m)	0.1
Dispersivity, primary direction (mobile) (α_1)	1 m
Dispersivity, secondary direction (mobile) (α_2)	0.1 m
Tortuosity factor (τ_L)	1
Coefficient of molecular diffusion (D_L)	1×10^{-6} m^2/s
Initial solute concentration	85 mg/L
Injection concentration	16,000 mg/L
Current driven	1 A/m
Mass transfer rate (β)	1×10^{-3}/day – 1×10^{-2}/day
Mobile porosity (Φ_m)	0.025
Immobile porosity (Φ_{im})	0.075
Dispersivity, primary direction (immobile, α_1)	0 m
Dispersivity, secondary direction (immobile, α_2)	0 m

Modeling Classical Advective-Dispersive Behavior

The fracture simulation using the advective-dispersive equation produces skewed solute arrival times, elongated tailing and a second peak (Figure 4). Notably, the discrete fracture results in hysteresis without the presence of diffusive mass transfer (Figure 5). The disequilibrium is a result of the difference in concentration in the fracture versus that in the surrounding matrix. Initially, solute moves rapidly through the fracture while solute in the surrounding matrix rock lags behind; the fluid EC is consequently high while the bulk EC is comparatively low because the rest of the volume supported by the bulk measurement still has a low solute concentration. In the storage phase, solute concentration in the fracture swiftly declines as the solute source is shut off, but solute in the matrix lags, resulting in a higher concentration outside the fracture. Hence, bulk apparent EC is greater than predicted from the fluid EC because solute concentrations in the matrix are now high compared to the fracture. The rapid removal of solute during the pumping phase leads to decreases in fluid and bulk apparent EC in the fracture and matrix. We observe a sharp increase in fluid EC in the fracture at the transition between storage and pumping phases, which suggests when pumping begins, solute is rapidly advected through the fracture zone resulting in an increase in observed fluid EC. The bulk apparent EC continues to decrease during pumping, but otherwise, the bulk apparent EC data mimic the breakthrough data. Macroscopic heterogeneity of sufficient magnitude and spatial extent produces hysteresis.

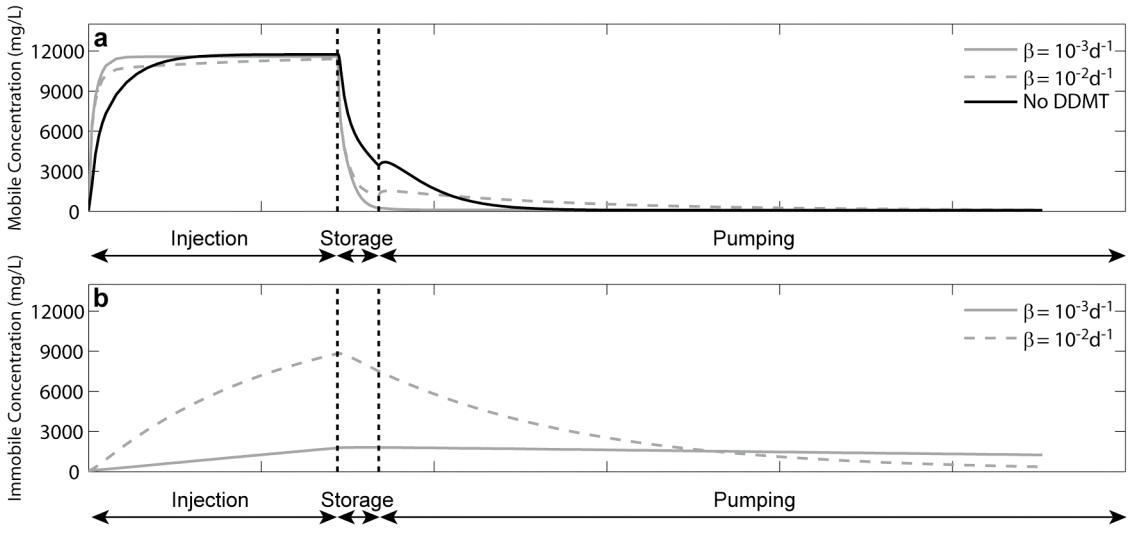

Figure 5: (a) Mobile and (b) immobile concentrations from a point within the discrete fracture. Without dual-domain mass transfer, concentration rebound is observed at the beginning of the pumping period due to solute being pulled back through the fracture. Introducing dual-domain mass transfer (thus lowering the mobile porosity from 0.1 to 0.025, in these models) hastens solute arrival times. With dual-domain mass transfer, lower peak concentrations and longer tails are observed. (c) Mobile domain concentrations for models with a homogenous mass transfer rate versus those with differing mass transfer rates between the matrix and fracture are nearly identical.

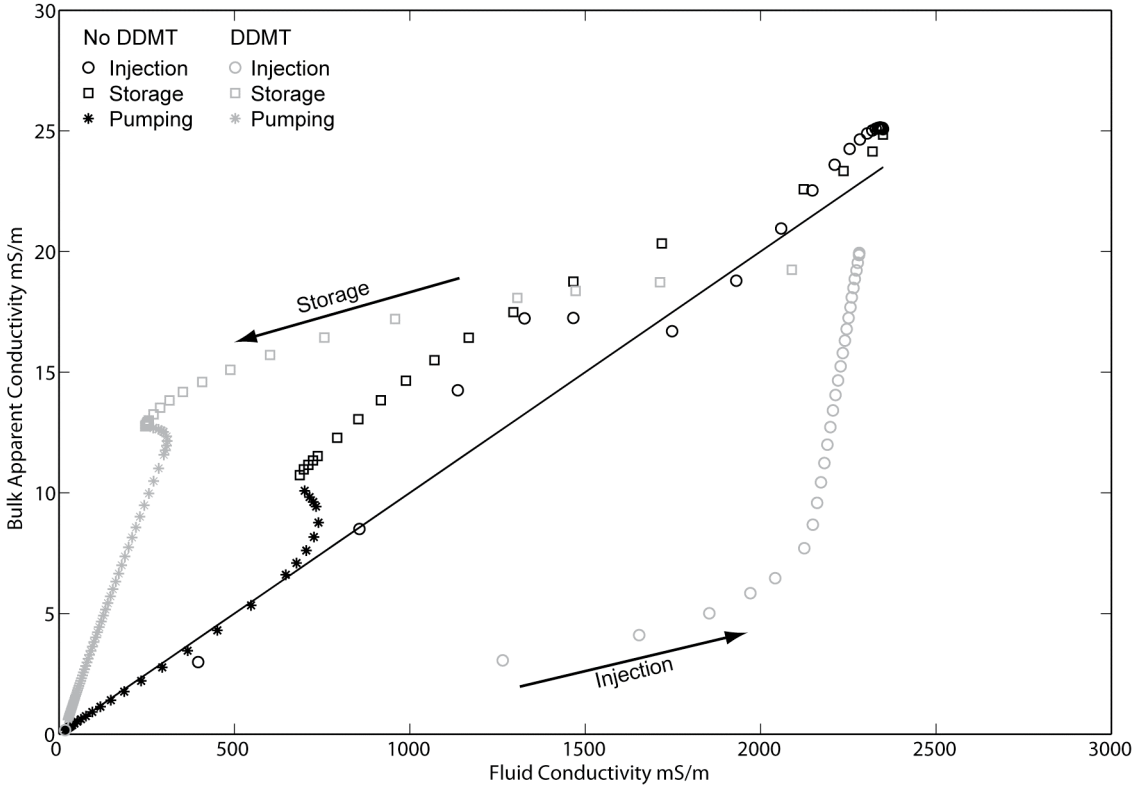

Figure 6: Simulated bulk apparent and fluid EC for a point within the discrete fracture. The black line is the true relation between bulk apparent and fluid EC used in the model. Discrete fracture zones result in hysteresis between bulk and fluid EC without explicitly invoking mass transfer processes (black symbols). Introducing dual-domain mass transfer increases the hysteresis (grey symbols). During the injection period, the hysteresis curve in the presence of dual-domain mass transfer is below the true relation between fluid and bulk apparent EC because

Figure 6: Simulated bulk apparent and fluid EC for a point within the discrete fracture. The black line is the true relation between bulk apparent and fluid EC used in the model. Discrete fracture zones result in hysteresis between bulk and fluid EC without explicitly invoking mass transfer processes (black symbols). Introducing dual-domain mass transfer increases the hysteresis (grey symbols). During the injection period, the hysteresis curve in the presence of dual-domain mass transfer is below the true relation between fluid and bulk apparent EC because the immobile domain (7.5% porosity) is relatively fresh compared to the mobile domain (2.5% porosity).

Modeling Dual-Domain Mass Transfer

Taking the numerical model above with a discrete fracture, we add dual-domain mass transfer by assigning an immobile porosity of 0.075, a mobile porosity of 0.025, and a mass transfer rate of 10^{-2}/day to both the fracture and matrix. The shape of the breakthrough curve for this scenario differs from the case of the discrete fracture without dual-domain mass transfer in two main ways (Figure 4): (1) solute concentrations during the injection and storage phases in the mobile domain for this case are lower than in the case without dual-domain mass transfer, which is expected because solute is being transferred into the immobile domain; and (2) this case creates a concentration history with a much more elongated tail than occurs considering advection-dispersion alone. We also observe hysteresis between fluid and bulk EC, but this curve differs from the case where no diffusive mass transfer occurs by having a larger lag between fluid and bulk apparent EC, the lag persists throughout both storage and pumping periods, and a lower bulk electrical conductivity during injection (Figure 5). The kink in the hysteresis curve at the transition between storage and pumping phases remains, as it is an advective effect between the fracture and matrix.

We also tested two cases where the fracture and matrix had different mass transfer rates. In one model, the matrix had a transfer of 1 x 10^{-3}/day (approximating a length scale of mass transfer of ~9 m) while the fracture had a mass transfer rate of 1 x 10^{-2}/day (approximating a length scale of mass transfer of ~3 m), while in the second model the rate of mass transfer in the matrix was 1 x 10^{-2}/day, and the rate of transfer in the fracture was 1 x 10^{-1}/day (approximating a length scale of mass transfer of 0.9 m). Increasing the mass transfer rate in the fracture by an order of magnitude beyond that used in the matrix resulted in breakthrough and EC behavior similar to the models with a single rate of mass transfer. EC and breakthrough behaviors were similar based upon the mass transfer rate in the matrix of the models, suggesting that the mass transfer rate of the matrix controls the observed hysteresis.

The disequilibrium produced by models with and without diffusive mass transfer are different when compared side-by-side. The disequilibrium caused by the fracture alone occurs over a shorter time-span and is smaller in magnitude, indicative of the small scale of mass transfer assumed. The lag caused by the advective effects of the fracture is imprinted upon the disequilibrium caused by dual-domain mass transfer, and manifests as a wider, smooth hysteresis that starts in the injection period and persists throughout the storage and pumping periods, indicative of both this small-scale mass transfer, and disequilibrium created by the presence of the 0.2 m-wide fracture.

Development of a Heterogeneous Hydraulic Conductivity Model

To explore the impact of dual-domain mass transfer on electrical signatures given a different type of heterogeneity, we develop a heterogeneous hydraulic conductivity model based on sequential Gaussian simulation. SGSIM [*Deutsch and Journel* 1998] was used to create a random hydraulic conductivity field 27 m wide and 46 m tall with a grid spacing of 0.25 m which

was centered on the pumping and observation wells (Figure 6). The geometric mean of the hydraulic conductivity is 5.96 x 10^{-4} m/s and the variance of the natural log of the hydraulic conductivity is 1.2. The hydraulic conductivity is set at 1.15 x 10^{-4} m/s throughout the rest of the model domain. The hydraulic conductivity field was then interpolated to the mesh, which contained 9890 elements. The model geometry and all other parameters are identical to those used in the homogeneous model. Modeling parameters are summarized in Table 3.

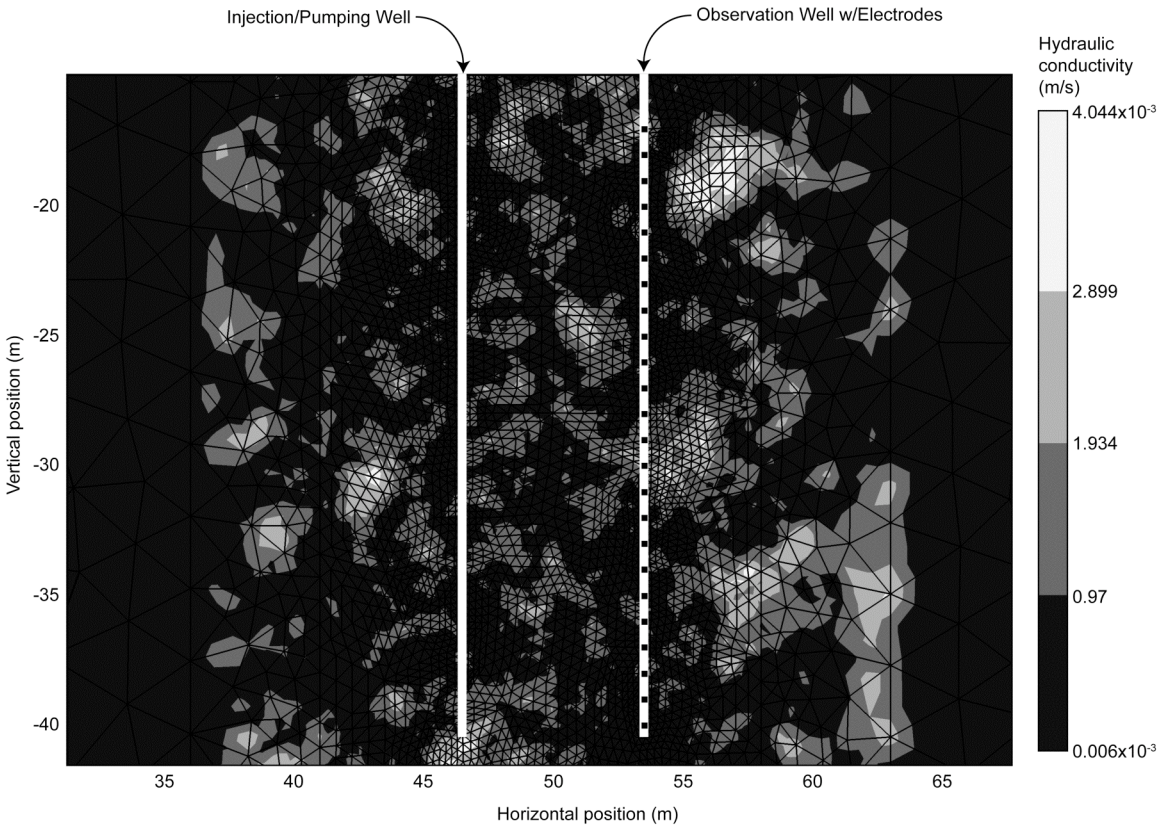

Figure 7: Inner part of mesh used in the heterogeneous K-field simulations. Pumping/injection and observation well locations are white and electrodes are represented with black rectangles.

Table 3: Physical parameters used in the heterogeneous numerical models of flow, transport, and electrical conduction.

Storage term (S)	3 x 10^{-5} m^{-1}

Modeling Classical Advective-Dispersive Behavior

When considering advective-dispersive behavior in this heterogeneous field, the tracer breakthrough appears non-Fickian (Figure 7). Plume snapshots indicate preferential fluid pathways, which are expected given the variations in the hydraulic conductivity. The bulk apparent EC data also indicates preferential fluid pathways. While more subtle than the discrete fracture case without mass transfer present, the relation between the bulk apparent and fluid EC exhibits hysteresis (Figure 8). As seen in the fracture modeling, macroscopic heterogeneity produces hysteresis associated with the variability in hydraulic conductivity alone.

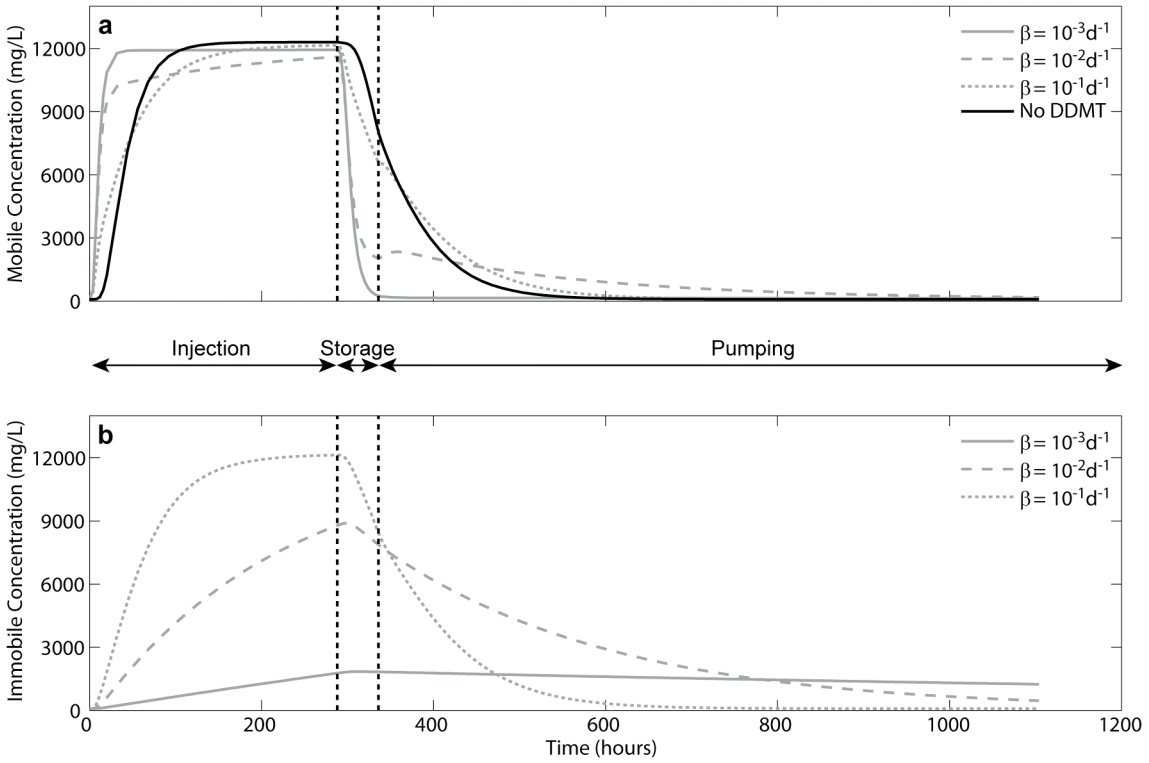

Figure 8: (a) Mobile and (b) immobile concentration at one point in space from the model with

immobile domains approach equilibrium and concentration behavior is similar to the single domain case. Intermediate transfer rates result in deviation from equilibrium behavior such as the rebound observed at the beginning of the pumping period. With dual-domain mass transfer, mobile domain concentration peaks are lower and longer tails are observed.

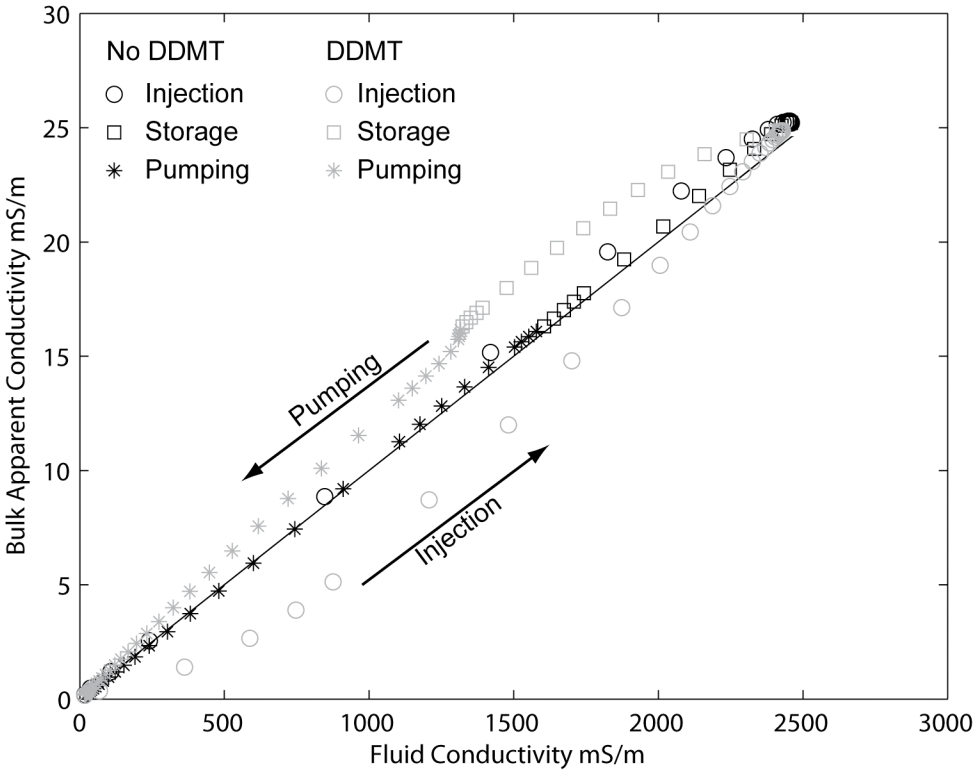

Figure 9: Simulated bulk apparent and fluid EC for a model with heterogeneous hydraulic conductivity. The black line is the true relation between bulk apparent and fluid EC used in the model. Heterogeneity in hydraulic conductivity (var(ln(K) = 1.2), without dual domain mass transfer, results in a slight hysteresis between fluid and bulk apparent EC without invoking mass transfer processes explicitly (black symbols). The addition of dual-domain mass transfer at a rate of 10^{-1}/day (grey symbols) increases the hysteresis, as would be expected. The hysteresis observed here is smaller than the previous two cases because the high rate of mass transfer keeps the mobile and immobile domains closer to equilibrium.

Modeling Dual-Domain Mass Transfer

Given the model above, we now add mass transfer by assuming an immobile porosity of 0.075, a mobile porosity of 0.025, and a range of mass transfer rates. Breakthrough curves exhibit longer tails due to solute that has been transferred into the immobile domain (Figure 7). As the mass transfer rate increases, the amount of solute transferred into the immobile domain and the length of time it is held there increases. Plume snapshots still indicate preferential pathways from the permeability heterogeneity. Notably, areas of lower hydraulic conductivity have a higher bulk apparent EC for longer time periods because these areas allow the mobile and immobile zones more time to transfer solutes. Again, we observe hysteresis curves caused by dual-domain mass transfer with the effects of larger-scale heterogeneity imprinted upon them (Figure 8). With mass transfer rates greater than 1×10^{-3}/day (representative of a length scale of mass transfer of ~9 m), we observe a rebound in concentration in the breakthrough and EC curves at the beginning of the pumping period caused by solute being transferred back into the mobile domain. When the mass transfer rate is increased to 10^{-1}/day (representative of a length scale of mass transfer of 0.9 m), the lag between mobile and immobile domains decreases and the system begins to appear more similar to a single domain case.

Discussion and Model Relevance to Field Studies

Our modeling demonstrates that macroscopic heterogeneity as well as solute mass transfer create hysteresis between bulk apparent and fluid EC data, and that the magnitude of hysteresis is a function of the scale of solute mass transfer. While separating advective and diffusive behavior may be difficult in field data, the disconnect between fluid and bulk EC data could be used to estimate properties like mass transfer rates or the volume of immobile pore space. However, to analyze these values in a meaningful way would require an understanding of the site geology and expected heterogeneity. For example, fractures sets can occur as groups of tens to thousands of individual fractures in the field; it is therefore likely in highly fractured media that the magnitude of hysteresis is smaller than in cases where only a small proportion of large-scale fractures may be relevant for conducting fluids [*Long et al.* 1991; *Renshaw* 1995; *Hsieh and Shapiro* 1996]. Based on our model results, we conclude that the shape of the hysteresis curve in field settings tells us about variations in the length scales of heterogeneity controlling transport.

We should note that these models cannot be fully representative of field processes, in part because of the dimensionality of the modeling, but also because field data are complicated by the effects of fine-scale heterogeneity in hydraulic conductivity or mass transfer parameters, which are not considered here. For example, we chose to use a single rate of mass transfer in our models, although many other studies have utilized multiple rates of mass transfer. Quantification of mass transfer processes at multiple scales in field settings may be possible, but would be dependent on collecting multiscale geophysical data. We also note that the time-scale of observation affects the role that heterogeneity played in producing hysteresis between bulk and fluid EC. In the discrete fracture model, solute traveling strictly through the matrix broke through

at the observation well and the resulting difference between concentration in the matrix and fracture caused the observed hysteresis. If we reduced the model simulation time, solute moving strictly through the matrix would not have enough time to reach the observation well and the hysteresis caused by large-scale heterogeneity would be absent. Despite these simplifications, we can reproduce a disconnect between the fluid and bulk apparent EC similar to that observed by *Singha et al.* [2007] in the field given either macroscopic heterogeneity or small-scale mass transfer, and demonstrate that the disconnect is driven by the length scales of heterogeneity, which may be information that is exploitable in field settings.

Conclusions

Previous studies have highlighted the complexity associated with interpreting solute transport processes from limited measurements of point-scale fluid chemistry data, and that geophysical data may be useful in estimating mass transfer rates and immobile porosities in situ. Our modeling results indicate that subscale dual-domain mass transfer and macroscopic heterogeneity both produce a measurable hysteresis between fluid and bulk apparent EC. The hysteresis is controlled by the geometry of low permeability material, the mass transfer rate, and the aquifer porosity, which means that the curve shape is indicative of the length scale over which mass transfer is occurring.

While quantifying advective versus diffusively controlled transport can be ambiguous from these data, we note that the disequilbrium between fluid EC and bulk EC data is indicative of mass transfer processes at some scale, and provides a manner for estimating mass transfer rates between domains and the volume of immobile pore space as shown in *Day Lewis and Singha* [2008]. Collecting multiscale geophysical data may be key to determining how the rates of mass transfer change with scale. In cases where good information on site geology exists such that the macroscopic heterogeneity is well characterized, electrical measurements may be used to help discern advective versus diffusive controls on transport.

Appendix A: Future Work

One of the key points presented in this thesis is that hydraulic conductivity heterogeneity can produce hysteresis between fluid and bulk apparent EC. This suggests that the shape of the hysteresis tells us about the length scale at which mass transfer is important. What remains to be done is to use the hysteresis curves to quantify the significance of that length scale. *Day-Lewis and Singha* [2008] demonstrated theoretically that mass transfer parameters could be related to temporal moments of mobile and bulk concentrations. Using this process, mass transfer parameters could be found in a simulated, lab, or field test, and if the coefficient of molecular diffusion is known, then the length scale at which mass transfer is important could be inferred from the mass transfer rate. Because obtaining sufficient measurement of heterogeneity is difficult, developing geophysical tools to quantify the other parameters – such as diffusion length and mass transfer rate – that control the observed hysteresis is crucial to our ability to discern between advective and diffusive controls on solute transport.

Another step forward on this work would be to model systems containing multiple rates of mass transfer. Using a single rate of mass transfer was sufficient to show that macro-scale heterogeneity could produce a similar electrical signature to dual-domain mass transfer although with longer mass transfer rates, but multiple rates of mass transfer are likely in the field as immobile domains range in size from cracks in sand grains to macroscopic zones of low permeability. The numerical models presented here could be adapted to simulate geophysical data at multiple scales to investigate multiple rates of mass transfer. Electrical resistivity surveys can utilize a variety of electrode configurations, and thus support scales, to provide insight into mass transfer rates over multiple scales of investigation. Spectral induced polarization methods, which measure the amplitude and phase lag of the voltage change, may also have a role to play.

The results presented here should be tested with a field experiment to quantify the role of dual-domain mass transfer with differing heterogeneity, such as the MAcroDispersion Experiment, Mirror Lake, and Cape Cod sites. In the numerical analysis we conducted, bulk apparent EC varied only with concentration. In the field, variations in permeability and lithology will also contribute to the observed electrical signature. Additionally, thin conductive features – such as fractures – can complicate the collection and interpretation of geophysical data. To quantify how the scale of hydraulic heterogeneity and geophysical measurement affected the observed electrical signatures, we needed to address these effects. For instance, in the field, a suite of background fluid and bulk apparent EC data could be collected prior to solute injection and analyzed to identify background features. The findings presented here are applicable to cases involving conservative tracers. However, hydrologists frequently deal with environmental problems concerning reactive materials. To make this work more broadly applicable, we would need to quantify if chemical processes such as sorption, radioactive decay, and biodegradation have an electrical signature. Common environmental applications of electrical geophysics include monitoring landfill leachates and hydrocarbons. Any chemical that changes the ionic strength of the fluid will impact the electrical properties of the subsurface, but the magnitude of these changes is determined by the specific chemical(s) present. Assuming a chemical affects the subsurface electrical properties, adsorption onto the host material would take it out of the mobile zone, but not out of the bulk geophysical measurement which is sensitive to both the mobile and immobile zones. This could result in a discrepancy between fluid and bulk apparent EC similar to the electrical signature of dual-domain mass transfer. Chemical data might also be used to determine the portion of adsorbed material and the resulting EC change. Radioactive decay products will influence EC in proportion to the daughter products created, which we do not expect to result in hysteresis. Bacterial activity has also been associated with EC changes. Typically bacterial activity increases bulk apparent EC, although it is uncertain if the increase in

EC is due to the presence of many bacteria or the chemical processes they carry out. The relationship between bacterial activity and bulk apparent EC is still being investigated.

Appendix B: Using COMSOL Multiphysics for Modeling Coupled Systems

COMSOL is a finite-element code capable of solving partial differential equations applicable to a wide variety of physics phenomena. Specifically of use to this work are the Conductive Media DC application, which is well suited for observing the electrostatics of conducting materials from a direct-current source, and the Earth Science Module, which contains Darcy's Law and Solute Transport applications. The Darcy's Law and Solute Transport applications both required transient analysis whereas the Conductive Media DC application required a stationary analysis.

Setting up a coupled flow, transport, and electrical conduction model required numerous iterations to find a combination of conditions that accurately represented the system of interest and provided a stable solution. For the time-dependent solver, a relative tolerance of 1×10^{-2} (dimensionless) was used for both transient applications, while absolute tolerances of 1×10^{-2} and 1×10^{-4} (dimensionless) were used for the Darcy's Law and Solute Transport respectively. The stationary solver's absolute tolerance was 1×10^{-6} for the Conductive Media DC application. The flow and transport problems were solved simultaneously (strongly coupled) using the UMFPACK direct solver. After these two simulations were finished, the steady-state electrical equation was solved for at each specified time-step for all the different electrode configurations with the UMFPACK solver.

Here, I outline some problems using COMSOL Multiphysics that might help others as they create models using this program. For example, the solute transport application would not solve initially because of the way the solution was passed between the Darcy's Law and Solute Transport applications. Under the Solver Parameters menu, the time steps to store as output were specified as "time steps from solver." At times in a transient model when there is an

instantaneous change, the solver takes very small time steps to resolve the change. These time steps can become so small compared to the time-keeping precision that they are labeled as the same time step (ex: t = 0.996(1), t = 0.996(2), etc.). When these time steps are passed to the next application, the solver cannot match each of these solutions to the problem it is currently solving i.e. the Solute Transport solution at time 0.996 seconds can be matched to either the Darcy's Law solution at time 0.996(1) or 0.996(2), but not to both. To avoid this, we set the time steps to store as output to be "specified times" which are input by the user.

The time steps taken by the solver contributed to other problems. By default, the solver is "free", meaning that there is no limit on the size of the time steps it takes. To prevent the solver from skipping over important events associated with flux changes at the injection/pumping well, we changed the time steps taken by solver option to "intermediate." This restricts the solver so that it must take at least one time step between each specified output time, but it is free to choose exactly when to take that step or to take more time steps if need be.

We also had problems solving the solute transport application due to difficulty resolving the instantaneous introduction of a large concentration source. Initially, it appeared as though the direct UMFPACK solver was the problem because the solute transport application could be solved with the iterative GMRES solver. The real issue was that we simulated the injection with a step function, which caused the time-stepping algorithm to not converge. Regardless of the solver used, we needed to use a smooth function to resolve injecting a large concentration. We applied a lag or inertia effect in the model by setting the heaviside scaling factor, which is a scalar variable in the Physics menu, to 100 seconds. This is a short amount of time compared to the total 1100 simulated hours and does not decrease model accuracy, but allows the model an allotted time to smooth out the injection.

Another complication came from adding the random hydraulic conductivity field to our simulations. By default, the solute transport application assumes that the velocity field is

divergence free, which means that the inflow minus outflow for a given element is zero at any time. The variations in fluid velocity resulting from hydraulic heterogeneity cause the total fluid flux for an element to not be zero. This condition violates the above assumption resulting in negative solute concentrations at early times, and concentrations that exceeded the injection concentration at late times. To conserve mass, we use the conservative form of the solute transport equation:

$$\mathbf{\Phi}_m \frac{\partial c_m}{\partial t} + \nabla \cdot (-\mathbf{\Phi}_m D_L \nabla c_m + \mathbf{u} c_m) = R_L . \tag{B1}$$

Note that the fluid velocity vector is now on the left-hand side of the equation rather than the right-hand side as in equation 3, which means that the divergence of the velocity vector may not be zero. By using the conservative form of the solute transport equation, we have stated that no solute may leave the model domain unless a flux condition is identified. For the pumping well to act as solute sink, we must specify the solute flux out as the concentration at that point multiplied by the fluid flux. At this time, we also began using the direct PARDISO solver to solve the coupled flow and transport applications because it is more time efficient for this problem than the other direct solvers. The UMFPACK solver solved the coupled fluid flow and solute transport problem in approximately 1.5 hours; the PARDISO solver takes roughly one third that time. Using the PARDISO solver and conservative form of the solute transport equation eliminated problems seen when using low hydraulic conductivity systems as well.

I additionally note that there are multiple ways to solve coupled applications. Several methods existed to solve the flow, transport and electrical conduction application models:

1) Solve each application sequentially. The advantage to this method is that we could use the solver for each application that in our experience had proven the most time-efficient and accurate (i.e. UMFPACK for the Darcy's Law and Electrical Conduction applications, and GMRES for the Solute Transport Application). Additionally, we could solve the Darcy's Law and

Solute Transport applications as time dependent, while maintaining the Electrical Conduction as steady-state. The disadvantage to this approach is that when solving transient applications, the variable being solved for is only written at each specified output time. Intermediate steps used by the solver for that application are not available when solving the next application. The loss of this data results in a less accurate solution.

2) Solve all the applications simultaneously (strongly coupled). The large concentration changes caused a rapidly evolving voltage field. To solve the electrical conduction application in this manner required increasing the relative solver tolerance from 10^{-2} to a minimum of 10 V to handle these changes. If the relative solver tolerance was below 10 V, which we considered to be too high, the model did not converge. In addition, the electrical conduction problem is best represented with a steady-state solution, and would have to be solved in a transient manner if the applications were solved simultaneously.

3) Combine the above approaches. By solving the transient flow and transport models as strongly coupled and then passing the solution at each time step to the steady-state electrical conduction model, we maintained a high degree of accuracy for all three parts of our model. Moreover, COMSOL may be interfaced with Matlab. We used this feature to script a solver routine that solved the electrical conduction application at each time step for a set of electrode configurations as would be used in a field electrical resistivity survey. The basic script structure is as follows:

- Generate model geometry
- Generate mesh
- Assign physical parameters (hydraulic conductivity, solute fluxes, boundary conditions, etc.)
- Solve couple fluid flow and solute transport problem
- Save fluid flow and solute transport solution

- Loop: create new electrode configuration
    - Loop: instruct the Conductive Media DC solver which time step of the Solute Transport solution to use
    - Assign physical parameters (electrical conductivity, solute distribution, boundary conditions, etc.)
    - Solve the Electrical Conduction problem
    - Store voltage data
    - End loop when last time step has been solved
    - Export voltage data
- End loop when last electrode configuration has been solved

An example script file for the homogeneous model with dual-domain mass transfer is shown in Appendix C, and follows the structure above.

Appendix C: Scripting a Homogeneous Dual-Domain Mass Transfer Model

The following is a Matlab script that solves a homogeneous hydraulic conductivity model with a single rate of dual-domain mass transfer for 21 different electrode configurations. The period of interest is 1100 hours. For those unfamiliar with Matlab, I would like to make note of a typographical convention. Any characters on the same line that follow a '%' are comments. They are not commands and are not executed by the code; rather they are text input by the writer to serve as a reminder, explanation, or other form of aid in deciphering code for the user. I also note that there is a very easy way to create the scripts. One can create the numerical model using the COMSOL GUI, then save it as a Matlab script file and edit as desired. This can be done by going to the File menu, and selecting Save As. The default file type is .mph, change this to model m-file or .m to save the model as a Matlab script instead. When scripts are created this way, COMSOL does not include variables that remain as the default value. For example, because we used the default dispersivity in the primary flow direction in the Solute Transport application that represents the mobile domain, it does not appear as an explicit entry in the Matlab script. Also, COMSOL works in base SI units which means that variables defined in Tables 1, 2, and 3 have to be converted into base SI before being entered into COMSOL or the Matlab script.

The Matlab script is as follows:

```
% The commands that create the model geometry go here.  They are omitted
% due to space considerations.

% Initialize mesh
fem.mesh=meshinit(fem, ...
'hauto',7, ...      % The number here defines the default mesh size, in this case
                    % "coarser", relative to the size of the domain.
   'point',[], ...
   'edge',[], ...
   'subdomain',[3]);   % This indicates which part of the geometry to mesh.
```

```
% Refine mesh
fem.mesh=meshrefine(fem, ...
   'mcase',0, ...
   'rmethod','regular', ...
   'subdomain',[3]);

% Refine mesh
fem.mesh=meshrefine(fem, ...
   'mcase',0, ...
   'rmethod','regular', ...
   'subdomain',[3]);

% Initialize mesh
fem.mesh=meshinit(fem, ...
   'hauto',7, ...
   'point',[], ...
   'edge',[], ...
   'subdomain',[2], ...
   'meshstart',fem.mesh);

% Initialize mesh
fem.mesh=meshinit(fem, ...
   'hauto',7, ...
   'point',[], ...
   'edge',[], ...
   'subdomain',[1], ...
   'meshstart',fem.mesh);

% (Default values are not included)

% Application mode 1
% Here we assign the physical properties of our first application, in this
% case the Darcy's Law application.
% The 'appl' or application commands are the basic options associated with
% this physics problem.
clear appl
appl.mode.class = 'Darcy';
appl.module = 'ES';
% The suffix below identifies all the variables in this application.
appl.assignsuffix = '_esdl';
clear prop
prop.variable='H';      % This is the variable the application solves for.
prop.analysis='time';   % This means the application is time dependent.
appl.prop = prop;
% 'pnt' commands assign the point properties.
clear pnt
% The order of the flux properties is matched to the order of the groups
% defined below.  For example, the first set of inner brackets for pnt.tNO
% is empty and correspond to Well 1, the values in the second set of inner
```

```
% brackets are associated with Well 3, and the following empty brackets
% correspond to the unnamed group ('').
pnt.tN0 = {{},{0;1209601},{}};  % Specify flux start times.
pnt.tNf = {{},{1036800;3974400},{}};    % Specify flux end times.
pnt.N0 = {{},{'2.19*10^-6';'-2.97*10^-6'},{}};  % Specify fluxes.
% Each name defines a group of points and has properties as specified above
pnt.name = {'Well 1','Well 3',''};
% pnt.ind indexes each point (there are 68 in this model) in order.  The value
% in the index corresponds to a set of the brackets in the variables above.  For example, the first
% value in pnt.ind is 1.  This means that the value of a pnt variable (such as pnt.tN0) at point 1 is
% equal to the value in the first set of brackets (in this case no value is assigned).  If the value in
% pnt.ind is 2, then the values at that point are defined as the values in the second set of brackets.
% Point 7 for example has a value of 2 in pnt.ind which means that point 2 has a flux of
% 2.19*10^-6 that starts at time 0 and ends at time 1036800, then a second flux of -2.97*10^-6
% from time 1209601 to time 3974400.  Boundary and subdomain properties are assigned the
% same way.
pnt.ind = [1,1,3,3,3,3,2,2,2,2,2,2,2,2,2,2,2,2,2,2,2,2,2,2,2,2,2,2,2,2,2,2, ...
   2,2,2,2,2,2,2,2,1,1,1,1,1,1,1,1,1,1,1,1,1,1,1,1,1,1,1,1,1,1,1,1,3,3,3, ...
   3,1,1];
appl.pnt = pnt;
% 'bnd' commands assign boundary properties.
clear bnd
% We use 3 different boundary conditions: HO = specified head, Nz = no
% flow, and cont = continuous or internal.
bnd.type = {'H0','Nz','cont','H0'};
% The head values associated with each boundary condition.
bnd.H0 = {3,0,0,1};
bnd.ind = [1,2,2,3,3,2,3,3,2,3,2,3,2,4];
appl.bnd = bnd;
% 'edu' commands assign subdomain properties.
clear equ
equ.S = '3*10^-5';  % Storage term
equ.Ks = .000115;   % Hydraulic conductivity
% Indicates that there are 3 subdomains all using the same settings.
equ.ind = [1,1,1];
appl.equ = equ;
appl.var = {'tscale','100'};    % Heaviside scaling factor
fem.appl{1} = appl;

% Application mode 2
% Assign physical properties for the Solute Transport application.  This
% application represents the mobile domain.
clear appl
appl.mode.class = 'SoluteTransSat';
appl.module = 'ES';
appl.assignsuffix = '_esst';
clear prop
prop.material='liquid';
prop.analysis='time';
```

```
clear weakconstr
weakconstr.value = 'off';
weakconstr.dim = {'lm2'};
prop.weakconstr = weakconstr;
appl.prop = prop;
clear pnt
% Empty brackets show that no value was entered
pnt.tc0 = {{{''}},0,{{''}},{{''}}};     % Specify concentration start time.
pnt.c0 = {{{''}},16,{{''}},{{''}}};     % Specify concentration
pnt.tcf = {{{''}},1036800,{{''}},{{''}}};   % Specify concentration end time.
pnt.name = {'Else','Well 3','Well 1',''};
pnt.ind = [1,1,4,4,4,4,2,2,2,2,2,2,2,2,2,2,2,2,2,2,2,2,2,2,2,2,2,2,2,2,2, ...
   2,2,2,2,2,2,2,2,3,3,3,3,3,3,3,3,3,3,3,3,3,3,3,3,3,3,3,3,3,3,3,4,4,4, ...
   4,1,1];
appl.pnt = pnt;
clear bnd
% Boundary types are specified concentration, no flux, continuous or
% internal, and advective flux.
bnd.type = {'C','Nn','cont','Na'};
bnd.c0 = {.085,0,0,0};
bnd.ind = [1,2,2,3,3,2,3,3,2,3,2,3,2,4];
appl.bnd = bnd;
clear equ
equ.DmL = .000001;  % Coefficient of molecular diffusion
equ.init = .085;    % Initial solute concentration
equ.v = 'v_esdl';   % Velocity in the y-direction
equ.u = 'u_esdl';   % Velocity in the x-direction
equ.theta_s = .025; % Mobile domain porosity
equ.alpha2 = .1;    % Dispersivity - secondary direction
% The reaction term is specified as the mass transfer rate (in units of 1/s) multiplied by the
% difference in concentration between the mobile and immobile domain
equ.RL = '(-1.157*10^-8)*(c-c2)';
equ.ind = [1,1,1];
appl.equ = equ;
appl.var = {'tscale','100'};    % Heaviside scaling factor
fem.appl{2} = appl;

% Application mode 3
% Assign physical properties for the Conductive Media DC application.
% Even though we are not solving for it yet, we must define the physical
% properties.
clear appl
appl.mode.class = 'ConductiveMediaDC';
appl.assignsuffix = '_dc';
clear prop
clear weakconstr
weakconstr.value = 'off';
weakconstr.dim = {'lm4'};
prop.weakconstr = weakconstr;
```

```
appl.prop = prop;
clear pnt
pnt.Qj0 = {0,-1,1}; % Electrical current values
pnt.ind = [1,1,1,1,1,1,1,1,1,1,1,1,1,1,1,1,1,1,1,1,1,1,1,1,1,1,1,1,1,1,1, ...
    1,1,1,1,1,1,1,1,3,1,2,1,1,1,1,1,1,1,1,1,1,1,1,1,1,1,1,1,1,1,1,1,1,1,1, ...
    1,1,1];
appl.pnt = pnt;
clear bnd
% Boundary types are specified voltage and continuous or internal
bnd.type = {'V','cont'};
bnd.ind = [1,1,1,2,2,1,2,2,1,2,1,2,1,1];
appl.bnd = bnd;
clear equ
% Electrical conductivity
equ.sigma = '1*(.025+.075)^1*(.025*.2*c+.075*.2*c2)';
equ.ind = [1,1,1];
appl.equ = equ;
fem.appl{3} = appl;

% Application mode 4
% Assign physical properties for the immobile domain.
clear appl
appl.mode.class = 'SoluteTransSat';
appl.dim = {'c2'};
appl.name = 'esst2';
appl.module = 'ES';
appl.assignsuffix = '_esst2';
clear prop
prop.material='liquid';
prop.analysis='time';
clear weakconstr
weakconstr.value = 'off';
weakconstr.dim = {'lm3'};
prop.weakconstr = weakconstr;
appl.prop = prop;
clear bnd
bnd.type = {'Nn','cont','C','Na'};
bnd.c0 = {0,0,.085,0};
bnd.ind = [3,1,1,2,2,1,2,2,1,2,1,2,1,4];
appl.bnd = bnd;
clear equ
equ.alpha1 = 0;     % Dispersivity in the primary flow direction
equ.DmL = .000001;
equ.init = .085;
equ.theta_s = .075;
equ.alpha2 = 0;
equ.RL = '-(-1.157*10^-8)*(c-c2)';
equ.ind = [1,1,1];
appl.equ = equ;
```

```
appl.var = {'tscale','100'};
fem.appl{4} = appl;
fem.frame = {'ref'};
fem.border = 1;
fem.outform = 'general';
clear units;
units.basesystem = 'SI';
fem.units = units;

% Multiphysics
fem=multiphysics(fem);

% Extend mesh
fem.xmesh=meshextend(fem, ...
   'linshape',[]);

% Solve coupled flow, transport and dual-domain mass transfer problem.
fem.sol=femtime(fem, ...
   'solcomp',{'c2','c','p'}, ...   % Specify the variables to solve.
   'outcomp',{'c2','c','p','V'}, ...   % Specify the solutions to output.
   'tlist',[0:14400:72000 115200:43200:1022400 1026000:3600:1051200
1065600:14400:1195200 1198800:3600:1224000 1238400:14400:1296000
1339200:43200:3974400], ...   % Specify the list of times
   'atol',{'p','.01','c','.0001'}, ... % Set the absolute tolerance.
   'tout','tlist'); % Specify the solution output times as the list above.

% Save current fem structure for restart purposes
% Save as fem2 (which is not the default) to ensure that the concentration
% solutions are not overwritten by other data.
fem2=fem;

% Define x coordinates of concentration output
x = [53.5 53.5 53.5 53.5 53.5 53.5 53.5 53.5 53.5 53.5 53.5 53.5 53.5 53.5 53.5 53.5 53.5 53.5 53.5 53.5
53.5 53.5 53.5];
% Define y coordinates of concentration output
y = [-18.5 -19.5 -20.5 -21.5 -22.5 -23.5 -24.5 -25.5 -26.5 -27.5 -28.5 -29.5 -30.5 -31.5 -32.5 -33.5
-34.5 -35.5 -36.5 -37.5 -38.5];
% Define output times of concentration data
time = [0:14400:72000 115200:43200:1022400 1026000:3600:1051200 1065600:14400:1195200
1198800:3600:1224000 1238400:14400:1296000 1339200:43200:3974400];

% Extract concentration data at all solution times at specified
% coordinates.
[Time,Conc] = postinterp(fem2, 't', 'c', [x;y], 'solnum', 'all');
% Create a variable with the concentration data, coordinates, and list of
% output times.
conc = [0,0,time; x', y', Conc'];
% Save the variable as an ascii file with tab delimiters.
save concA1RLMT.txt conc -ascii -tabs
```

```
% (Default values are not included)

% Loop to solve multiple electrode configurations.  We will solve for 21
% different skip 0 configurations, so we have a loop that iterates 21
% times.
for i = 1:21
   % The electrodes are represented by points 39 through 62 in the model.
   % This was identified by accessing the physics, then point settings
   % menu in the COMSOL GUI.  We are simulating a dipole-dipole array
   % which means that the first electrode is the current source, and the
   % second electrode is the current sink.  Our electrode array begins at
   % the bottom of the well which corresponds to point 39.  This means
   % that over all the iterations, points 39 - 59 will be current sources
   % and points 40 - 60 will be current sinks.  There are a total of 68
   % points in the model.
   % Creat a new point index for the Conductive Media DC application.
   points = ones(1,68);
   points(1,i+38) = 3;     % Assign the current source.
   points(1,i+39) = 2;     % Assign the current sink.

   % Define parameters needed to extract data
   % Define x coordinates
   x = [53.5 53.5 53.5 53.5 53.5 53.5 53.5 53.5 53.5 53.5 53.5 53.5 53.5 53.5 53.5 53.5 53.5 53.5 53.5 53.5
53.5 53.5 53.5 53.5 53.5 53.5 53.5];
   % Define y coordinates
   y = [-17 -18 -19 -20 -21 -22 -23 -24 -25 -26 -27 -28 -29 -30 -31 -32 -33 -34 -35 -36 -37 -38 -39
-40];
   % Define time step (needed to label final output)
   time = [0:14400:72000 115200:43200:1022400 1026000:3600:1051200
1065600:14400:1195200 1198800:3600:1224000 1238400:14400:1296000
1339200:43200:3974400]';

   % This loop passes the flow and transport solution from each time step
   % to the Conductive Media DC application.  The time list we specified
   % above contains 121 steps.
   for j = 1:121

      % Again, we have to define the physics for each application.
      % Because the flow and solute transport physics are the same as
      % above, they are omitted here.

      % Application mode 3
      clear appl
      appl.mode.class = 'ConductiveMediaDC';
      appl.assignsuffix = '_dc';
      clear prop
      clear weakconstr
      weakconstr.value = 'off';
```

```
weakconstr.dim = {'lm4'};
prop.weakconstr = weakconstr;
appl.prop = prop;
clear pnt
% Note here that for the index of points, a value of 1 means no
% current, 2 means it is a current sink, and 3 means the point is
% a current source.
pnt.Qj0 = {0,-1,1};
pnt.ind = points;       % Here we change the point index to be the variable we defined.
appl.pnt = pnt;
clear bnd
bnd.type = {'V','cont'};
bnd.ind = [1,1,1,2,2,1,2,2,1,2,1,2,1,1];
appl.bnd = bnd;
clear equ
equ.sigma = '1*(.025+.075)^1*(.025*.2*c+.075*.2*c2)';
equ.ind = [1,1,1];
appl.equ = equ;
fem.appl{3} = appl;

% Multiphysics
fem=multiphysics(fem);

% Extend mesh
fem.xmesh=meshextend(fem, ...
   'linshape',[]);

% Evaluates initial values using current solution.
init = asseminit(fem,'u',fem2.sol);

% Evaluate the electrical conduction problem using the flow and
% transport solution at time j.
u = asseminit(fem,'init',fem2.sol,'solnum',j);

% Solving Conductive Media DC application.
fem.sol=femstatic(fem, ...
   'init',init, ...
   'u',u, ...
   'solcomp',{'V'}, ...
   'outcomp',{'c2','c','p','V'});

% Save current fem structure for restart purposes.
fem0=fem;

% Extract voltage data at desired coordinates.
[score] = postinterp(fem,'V',[x;y]);

% Data Storage
% If we are starting a new electrode configuration, then initialize
```

```
      % the temporary data matrix.  Otherwise concatenate the new data
      % onto the existing data.
      if j == 1
         volt = score;
      else
         volt = [volt;score];
      end
   end

   % Create matrix of voltage data with coordinates and times.
   Vdata = [0,x;0,y;time,volt];
   % Data file format:
   % row 1 = padded 0 then x data
   % row 2 = padded 0 then y data
   % rows 3 to end: first column is the times, rest are voltages aligned under proper
   % coordinates

   % Saves the voltage data in an ascii format with tab delimiters
   % in a text file.
   save (['A1rlmt',num2str(i),'.txt'],'Vdata','-ascii','-tabs')
end
```

References

Adams, E. E., and Gelhar, L. W., 1992. Field study of dispersion in a heterogeneous aquifer 2. Spatial moments analysis. *Water Resour. Res.*, **28** (12):3293–3307, doi:10.1029/92WR01757.

Archie, G. E., 1942. The electrical resistivity log as an aid in determining some reservoir characteristics: Transactions of the American Institute of Mining. *Metallurgical and Petroleum Engineers*, **146**:54-62.

Barlebo, H. C., Hill, M. C., and Rosbjerg, D., 2004. Investigating the Macrodispersion Experiment (MADE) site in Columbus, Mississippi, using a three-dimensional inverse flow and transport model. *Water Resour. Res.*, **40** (4):1-18, doi:10.1029/2002WR001935.

Bear, J., 1972. *Dynamics of Fluids in Porous Media*: Elsevier Publishing Company.

Becker, M. W., and Shapiro, A. M., 2000. Tracer transport in fractured crystalline rock: Evidence of nondiffusive breakthrough tailing. *Water Resour. Res.*, **36** (7):1677-1686, doi:10.1029/2000WR900080.

Becker, M. W., and Shapiro, A. M., 2003. Interpreting tracer breakthrough tailing from different forced-gradient tracer experiment configurations in fractured bedrock. *Water Resour. Res.*, **39** (1):1-13, doi:10.1029/2001WR001190.

Benson, D. A., Wheatcraft, S. W., and Meerschaert, M. M., 2000. The fractional-order governing equation of Levy motion. *Water Resour. Res.*, **36** (6):1413-1423, doi:10.1029/2000WR900032.

Berkowitz, B., and Scher, H., 1995. On characterization of anomalous dispersion in porous and fractured Media. *Water Resour. Res.*, **31** (6):1461-1466, doi:10.1029/95WR00483.

Berkowitz, B., and Scher, H., 2001. The role of probabilistic approaches to transport theory in heterogeneous media. *Transport in Porous Media*, **42** (1):241-263, doi:10.1023/A:1006785018970.

COMSOL Multiphysics User's Guide, 2006. Version 3.3: COMSOL AB, Burlington, MA, USA, 708 pp.

Cortis, A., and Berkowitz, B., 2004. Anomalous transport in "classical" soil and sand solumns. *Soil Sci Soc Am J*, **68** (5):1539-1548.

Day-Lewis, F. D., Lane, J. W., and Gorelick, S. M., 2006. Combined interpretation of radar, hydraulic, and tracer data from a fractured-rock aquifer near Mirror Lake, New Hampshire, USA. *Hydrogeology journal*, **14** (1):1-14, doi:10.1007/s10040-004-0372-y.

Day-Lewis, F. D., and Singha, K., 2008. Geoelectrical inference of mass transfer parameters using temporal moments. *Water Resour. Res.*, **44** (5):1-6, doi:10.1029/2007WR006750.

Dentz, M., and Tartakovsky, D. M., 2006. Delay mechanisms of non-Fickian transport in heterogeneous media. *Geophys. Res. Lett.*, **33** (16):1-5, doi:10.1029/2006GL027054.

Deutsch, C. V., and Journel, A. G., 1998. *GSLIB Geostatistical Software Library and User's Guide*: Oxford University Press, New York, 369 pp.

Feehley, C. E., Zheng, C., and Molz, F. J., 2000. A dual-domain mass transfer approach for modeling solute transport in heterogeneous aquifers: Application to the Macrodispersion Experiment (MADE) Site. *Water Resour. Res.*, **36** (9):2501-2515, doi:10.1029/2000WR900148.

Haggerty, R., and Gorelick, S. M., 1994. Design of multiple contaminant remediation: Sensitivity to rate-limited mass transfer. *Water Resour. Res.*, **30** (2):435-446, doi:10.1029/93WR02984.

Haggerty, R., and Gorelick, S. M., 1995. Multiple-rate mass transfer for modeling diffusion and surface reactions in media with pore-scale heterogeneity. *Water Resour. Res.*, **31** (10):2383-2400, doi:10.1029/95WR10583.

Harvey, C., and Gorelick, S. M., 2000. Rate-limited mass transfer or macrodispersion: Which dominates plume evolution at the Macrodispersion Experiment (MADE) Site? *Water Resour. Res.*, **36** (3):637-650.

Hill, M. C., Barlebo, H. C., and Rosbjerg, D., 2006. Reply to comment by F. Molz et al. on Investigating the Macrodispersion Experiment (MADE) site in Columbus, Mississippi, using a three-dimensional inverse flow and transport model. *Water Resour. Res.*, **42** (6):1-4, doi:10.1029/2005WR004624.

Hsieh, P. A., and Shapiro, A. M., 1996. Hydraulic characteristics of fractured bedrock underlying the FSE well field at the Mirror Lake Site, Grafton County, New Hampshire. *U.S. Geological Survey Toxic Substances Hydrology Program-Proceedings of the technical meeting, Colorado Springs, Colorado, September 20-24, 1993, U.S. Geological Survey Water-Resources Investigations Report 94-4015*:127-130.

Keller, G. V., and Frischknecht, F. C., 1966. *Electrical Methods in Geophysical Prospecting*: Pergamon Press, Oxford, U.K., 523 pp.

Levy, M., and Berkowitz, B., 2003. Measurement and analysis of non-Fickian dispersion in heterogeneous porous media. *Journal of Contaminant Hydrology*, **64** (3-4):203-226, doi:10.1016/S0169-7722(02)00204-8.

Long, J. C. S., Karasaki, K., Davey, A., Peterson, J., Landsfeld, M., Kemeny, J., and Martel, S., 1991. An inverse approach to the construction of fracture hydrology models conditioned by geophysical data : An example from the validation exercises at the Stripa Mine. *International Journal of Rock Mechanics and Mining Science & Geomechanics Abstracts*, **28** (2-3):121-142, doi:10.1016/0148-9062(91)92162-R.

Molz, F. J., Zheng, C., Gorelick, S. M., and Harvey, C. F., 2006. Comment on "Investigating the Macrodispersion Experiment (MADE) site in Columbus, Mississippi, using a three-dimensional inverse flow and transport model" by Heidi Christiansen Barlebo, Mary C. Hill, and Dan Rosbjerg. *Water Resour. Res.*, **42** (6):1-5, doi:10.1029/2005WR004265.

Renshaw, C. E., 1995. On the relationship between mechanical and hydraulic aperture in rough-walled fractures. *Journal of Geophysical Research*, **100** (B12):24629-24636.

Sánchez-Vila, X., and Carrera, J., 2004. On the striking similarity between the moments of breakthrough curves for a heterogeneous medium and a homogeneous medium with a matrix diffusion term. *Journal of Hydrology*, **294** (1-3):164-175, doi:10.1016/j.jhydrol.2003.12.046.

Singha, K., Day-Lewis, F. D., and Lane, J. W., Jr., 2007. Geoelectrical evidence of bicontinuum transport in groundwater. *Geophys. Res. Lett.*, **34** (12):1-5, doi:10.1029/2007GL030019.

Singha, K., and Gorelick, S. M., 2006. Effects of spatially variable resolution on field-scale estimates of tracer concentration from electrical inversions using Archie's law. *Geophysics*, **71** (3):G83-G91.

Singha, K., and Gorelick, S. M., 2006. Hydrogeophysical tracking of three-dimensional tracer migration: The concept and application of apparent petrophysical relations. *Water Resour. Res.*, **42** (6):1-14, doi:10.1029/2005WR004568.

Singha, K., Pidlisecky, A., Day-Lewis, F. D., and Gooseff, M. N., 2008. Electrical characterization of non-Fickian transport in groundwater and hyporheic systems. *Water Resour. Res.*, **44**:1-14, doi:10.1029/2008WR007048.

Slater, L., Binley, A. M., Daily, W., and Johnson, R., 2000. Cross-hole electrical imaging of a controlled saline tracer injection. *Journal of Applied Geophysics*, **44** (2-3):85-102, doi:10.1016/S0926-9851(00)00002-1.